DOI: 10.13009/EUCASS2019-373



# The confirmation of thermal boundary parameters of the Gas Oxygen Kerosene Rich Fueled rocket engine wall

*Zhixin Zhao *, Xianggeng Wei **, Lingyu Li, Xianggang Bian, Youxing Zuo*

*(Science and Technology on Combustion, Internal Flow and Thermo-structure Laboratory, Northwestern Polytechnical University, Xi'an 710072, China, *1138952399@qq.com*

*** realysnow@nwpu.edu.cn)*

**Abstract**

In this paper, theoretical analysis, numerical simulation and experimental testing methods will be used to study the thermal boundary conditions of the engine wall. Which is one of the key technologies in liquid engine design. The paper carried out an experimental study on a gas-oxygen kerosene liquid rocket with the oxy-fuel ratio of 1:1(the total flow of mass is 120g/s). The study shows that the heat flow calculated by the bartz formula(0.76 $MW/m^2$) is higher than the experimental value. However, the heat flow value calculated by the simulation of the gas thermal property parameters is the lowest (0.22 $MW/m^2$ at point3 and 0.24 $MW/m^2$ at point5). The main reason is that the numerical simulation ignores the effect of carbon deposition on heat transfer. The experiment measured 0.69 $MW/m^2$ at point3 and 0.74 $MW/m^2$ at point5, and found that carbon deposition can effectively reduce the heat transfer of gas to the wall. In the case of carbon deposition, the experimental results show that the heat flux values are respectively measured. It is 0.55 $MW/m^2$ and 0.27 $MW/m^2$, indicating that the closer to the engine outlet, the more serious the carbon deposition, and the lower the heat transfer efficiency of the gas to the wall.

**Key words:** heat flux, near wall gas temperature, gas wall surface temperature

## 1 .Introduction

Studying the thermal effect of gas on the engine wall plays a key role in the design of liquid rocket engines. However, due to the complexity of its mechanism, although countries have already carried out research on the heat transfer mechanism in the combustion chamber, especially the heat transfer mechanism between gas and solid, the mechanism of gas and engine wall action for each type of liquid rocket engine has not been systematically established so far. The model comes out, the existing model can only play a certain predictive role.

Lai et al. [1] studied the convective heat transfer between the inner wall of the combustion chamber and the gas and the flow of the coolant in the regenerative cooling channel by means of fluid-solid coupling numerical simulation. The interface between solid and fluid was treated by coupling wall. Wang Xiaowei et al [2,3] made a heat sink type combustion chamber using copper as the material, and used the thermocouple to obtain the inner wall temperature of the thrust chamber and the heat flow value of the gas to the wall surface. Combined with the unsteady numerical simulation of combustion in the combustion chamber, the internal flow field in the combustion chamber is obtained and compared with the experimental data. It is found that the calculation model is in good agreement with the

DOI: 10.13009/EUCASS2019-373



experimental results. Marco Pizzarelli et al. [4] established a two-dimensional model for liquid oxygen/methane engines (external runner cooling) and used simulations to estimate the internal gas flow, coolant flow and gas-to-wall heat transfer. The wall heat flow, gas temperature and gas sidewall temperature calculated by the Bartz formula are higher than the simulation results (about 10% to 20% higher), while the combustion chamber pressure is lower than the simulation results. In addition, the paper also found that only the two-dimensional result of the gas wall surface temperature is higher than the one-dimensional result, and other parameters (wall heat flow, gas temperature and combustion chamber pressure) are basically the same. Betti [5] established a model that can efficiently predict the wall temperature, heat flow and coolant pressure loss of regenerative cooling liquid rocket engines, and uses the CFD solver to calculate the two-dimensional model. The wall temperature is close to the experimental value. Celano [6] studied the heat transfer process of a gas-oxygen/methane propellant combination in a single-component coaxial shear nozzle combustion chamber. Through experimental measurements, and comparing the results with the one-dimensional simplified model, two-dimensional model and three-dimensional finite element and finite difference model calculation results, it is found that the one-dimensional model calculates the heat flow is high, and the three-dimensional results are the closest to the experiment. D. Suslov et al. [7] conducted experimental and numerical simulations on the heat transfer characteristics of the inner wall of the combustion chamber in the combustion chamber of liquid oxygen (LOX)/liquid methane (LCH4) rocket engine. By comparing the two cases of liquid film cooling and liquid film cooling, the heat flux of the gas to the gas wall is significantly reduced. The simulation results are consistent with the actual situation, the pressure deviation is less than 1%, and the heat flow deviation is larger, and higher than the experimental situation. Peter C. Ma et al. [8] proposed a flame-based combustion model to predict the heat transfer of the gas to the engine wall and the combustion of the cold wall against the combustion chamber. By setting the thermal boundary conditions, the flame structure under non-adiabatic conditions was obtained, and the performance of the model was analyzed by direct numerical simulation (DNS) to calculate the diffusion flame of hydrogen and oxygen under isothermal wall conditions. It is found through research that the model can predict the heat of gas, the composition of gas and the heat transfer of gas to the engine wall.

From the perspective of national studies, in the measurement and calculation of the near-gas wall surface temperature of the combustion chamber and the heat transfer heat flow of the gas to the wall, the experimental method is to arrange the thermocouple in the wall of the combustion chamber and test the temperature at different depths. Further derivation of the near gas wall surface temperature and the heat flow of the gas to the engine wall. The simulation method can be divided into group classification according to the different inlets, that is, the components of several gas are defined, regardless of combustion, and the components are mostly derived from the CEA calculation results; and the other is a single gas type, that is, the calculated gas is used. Physical parameters define a single gas for calculation. The last one is the combustion class, which is calculated by simplifying the consideration of the main step or the multi-step chemical reaction. In the theoretical calculation method, the Bartz formula is used more, and the method is mainly used to calculate the steady state heat flow value.

## 2. Zero-dimensional wall heat flow steady state calculation

The combustion inside the liquid rocket engine is more complicated, and the physicochemical properties of different regions are different. From the engine head to the nozzle, the combustion chamber can be divided into three regional atomization zones, evaporation zones and blending combustion zones. In order to simplify the theoretical calculation process, it is necessary to appropriately simplify the combustion process of the rocket, so the following assumptions are adopted:

(1) The gas is evenly distributed along the circumference of the engine;

(2) The gas is in a chemical equilibrium state in the combustion chamber;

DOI: 10.13009/EUCASS2019-373



(3) The gas component is evenly distributed along the axial direction and the radial direction, and the change of the pressure with the axial position is not considered.

## 2.1 Thermal calculation

The chemical reaction of the gas-oxygen/kerosene propellant combination engine is complicated, and there are many gas components, which can reach dozens. This paper uses the more mature NASA CEA (Chemical Equilibrium with Application) for calculation. The calculation was carried out using experimental conditions (fuel is JP10, oxidant is gas oxygen; combustion chamber condition is 17 bar; ratio is 1:1). The main parameters of the calculated gas are shown in Table 1. The main components of the calculated gas are shown in Table 2.

Table 1: Main physical property parameters of gas

| **the name of the parameters** | **the number of the parameters** |
|---|---|
| temperature $T_0$/K | 1764.65 |
| Pressure $p_c$/Pa | 1700000 |
| Characteristic velocity Cth*/m/s | 1471.19 |
| constant pressure specific heat ratio Cp/ (kj/(kg • K)) | 2.5637 |
| Prandtl number | 0.4824 |
| dynamic viscosity μ /(kg/(m • s)) | $5.75\times10^{-5}$ |
| specific heat ratio k | 1.2878 |
| density ρ（kg/m3） | 1.776 |

Table 2: Main components of gas

| **components** | **Mole fraction** |
|---|---|
| $H_2$ | 0.48413 |
| CO | 0.44640 |
| C(gr) | 0.06390 |
| $H_2O$ | 0.00134 |
| $CO_2$ | 0.00034 |

DOI: 10.13009/EUCASS2019-373



## 2.2 convective heat transfer

The convective heat transfer between the near wall gas and the engine wall is calculated using the relationship (1):

$$q_c = h_g\left(T_{aw} - T_{wg}\right) \tag{1}$$

$q_c$ is the heat flow per unit area of the gas flowing to the engine wall per unit area, W/m$^2$;
$h_g$ is the convective heat transfer coefficient of gas to engine wall, W / (m2 ·K);
$T_{aw}$ is the adiabatic wall temperature, because the speed in the combustion chamber is small, less than 0.3Ma, so the approximate treatment here is the gas temperature T0, K;
$T_{wg}$ is the gas side wall temperature in K.
The convective heat transfer coefficient is related to the composition and physicochemical properties of the gas. Different types of injectors will also cause different combustion types in the combustion chamber, which will lead to changes in the convective heat transfer coefficient. For the simplified calculation, the influence of factors such as combustion details is neglected, and the calculation model adopts the uniform gas hypothesis [9]. Di Lianshun et al. [10] proposed a near-experimental correction in his book "Rocket Engine Principles". The formula for calculating the convective heat transfer coefficient between the wall gas and the engine wall (2), namely the Bartz correlation:

$$h_g = \left[\frac{0.026}{d_t^{0.2}} \times \frac{\mu^{0.2} C_p}{\mathrm{Pr}^{0.6}} \times \left(\frac{p_c}{C_{th}^*}\right)^{0.8}\right]\left(\frac{A_t}{A}\right)^{0.9} \delta \tag{2}$$

$d_t$ is the throat diameter of the engine, the unit is m, where 0.012m is taken;
$A_t$ is the engine throat area, the unit is m2, here is $1.131\times10^{-4}$m$^2$;
A is the cross-sectional area of the combustion chamber, the unit is m2, here is $3.6\times10^{-3}$m$^2$;
δ is the correction coefficient established to introduce the influence of the change of the lateral airflow property of the boundary layer on the heat transfer coefficient. The calculation formula is as shown in (3):

$$\delta = \left[\frac{T_{wg}}{2T_0}\left(1 + \frac{k-1}{2}Ma^2\right) + \frac{1}{2}\right]^{-0.68}\left(1 + \frac{k-1}{2}Ma^2\right)^{-0.12} \tag{3}$$

Where k is the specific heat ratio of the gas; Ma is the Mach number in the combustion chamber, which is approximately 0.3.
Since the Bartz correlation is an empirical formula based on the turbulent boundary layer, the Reynolds number flowing in the combustion chamber should be calculated before use to analyze whether the internal flow is turbulent. The calculation formula is as shown in (4):

$$\mathrm{Re} = \frac{dV}{\nu} \tag{4}$$

d is the equivalent diameter of the inner cavity of the combustion chamber, the unit is m, here is 0.0667m;
V is the axial velocity of the gas, here is 333.09 m/s;

DOI: 10.13009/EUCASS2019-373



ν is the kinematic viscosity of the gas, expressed in $m^2/s$, calculated from μ/ρ and is $3.356\times10^{-5}m^2/s$.
It is calculated that the Reynolds number of the gas in the pipe is 672000, which is higher than 2300. Therefore, it is considered that the gas flow in the combustion chamber is turbulent, and it can be explained that the convective heat transfer coefficient can be solved by Bartz correlation.

### 2.3 Radiation heat transfer

The calculation of radiant heat flow is still based on the calculation formula of radiant heat flux density of uniform gas (5):

$$q_r = \varepsilon_{w,ef}\sigma\left(\varepsilon_g T_0^4 - a_w T_{wg}^4\right) \tag{5}$$

$q_r$ is the radiant heat flux density of the gas to the wall, in units of $W/m^2$;
$\varepsilon_{w,ef}$ is the effective blackness of the wall;
σ is the Stephen-Boltzmann constant with a value of $5.67\times10^{-8}$ $W/(m^2 \cdot K^4)$;
$\varepsilon_g$ is the gas blackness;
$a_w$ is the wall absorption rate.
The material used in the experimental engine of this study was 1Cr18Ni9Ti, so it was found that the blackness $\varepsilon_w$ of the material was 0.4[11].Estimate the effective blackness of the wall using the simplified formula (6), Substituting the data, the value is 0.3.

$$\varepsilon_{w,ef} = \frac{1-\varepsilon_w}{2} \tag{6}$$

The ability to emit and absorb radiation varies from one gas to another. For the components in the gas, monoatomic gases (O, H, etc.) and non-polarized diatomic gases ($H_2$, etc.) are not capable of emitting and absorbing radiation below 3000K, so the blackness of the gas is mainly affected by its internal polyatomic and polarized diatomic gases, namely $CO_2$, $H_2O$, and CO. At present, the main research is to consider only the radiation of $CO_2$ and $H_2O$. However, under the working conditions involved in this paper, the specific gravity of CO is very large. Therefore, in the treatment, the three gas components of $CO_2$, $H_2O$ and CO will be affected. In the calculation, the geometrical average of the blackness of $CO_2$, $H_2O$, and CO is used to represent the gas blackness, that is,

$$\varepsilon_g = \varepsilon_{H_2O} + \varepsilon_{CO_2} + \varepsilon_{CO} - \varepsilon_{H_2O}\varepsilon_{CO_2} - \varepsilon_{CO_2}\varepsilon_{CO} - \varepsilon_{CO}\varepsilon_{H_2O} + \varepsilon_{H_2O}\varepsilon_{CO_2}\varepsilon_{CO} \tag{7}$$

The last four terms in the formula are the result of taking into account that the overlapping portions of the spectra of the three gases $CO_2$, $H_2O$, and CO are mutually absorbed. The blackness values of the three gases $CO_2$, $H_2O$ and CO were obtained from the FLUENT database, which were 0.43, 0.54 and 0.17. The calculated blackness of the gas is 0.7824. It is assumed that the gas wall surface can be regarded as a diffuse gray body, that is, its absorption ratio and blackness are constant at a certain temperature, and the absorption ratio is consistent with the blackness at the same temperature [12].

DOI: 10.13009/EUCASS2019-373



### 2.4 Total heat flow calculation

The total heat flow of the gas to the engine gas wall side is the sum of the convective heat flow and the radiant heat flow(8). Assuming a gas wall surface temperature of 650 K, the total heat flow of the gas to the wall is 0.78 MW/m2, and the radiant heat flow accounts for 16.38% of the total heat flow (typically 15% to 20% [13]). The total convective heat transfer coefficient of the gas to the wall is 700 W/($m^2$ K).

$$q = q_c + q_r \tag{8}$$

## 3. Numerical simulation

### 3.1 Model simplification and numerical simulation

The experimental engine model is shown in Fig. 1. The model is simplified during the numerical simulation, which only the combustion chamber housing portion and its internal gas flow passage portion are considered, and the simplified model is in Fig. 2.

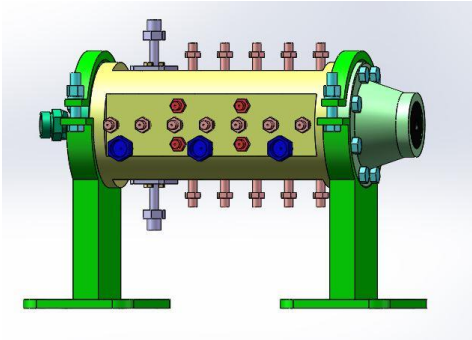

Figure 1: experimental engine modle

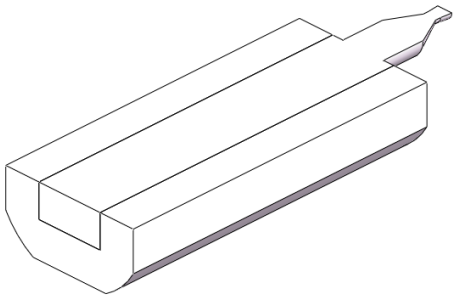

Figure 2: Simplified geometric model

There are four types of mesh for the simplified model: 0.35 million, 0.61 million, 1.08 million, and 1.62 million. The pressure values in the combustion chamber calculated by the four types of grids and the temperature curves on the midline of the interface at 20s are compared as shown in the figure5. It can be seen from the results that the pressure difference of these four types of grids is within 1%, and the temperature curves calculated by 1.08 million and 1.62 million grids are closer, the maximum temperature difference is 2.2%. (Constant gas thermal property parameter), 3.6% (fixed gas component). This shows that the calculation using the 1.08 million grid is the best.

From the temperature comparison curve of the two, it is easy to see that after the gas passes through the inlet, the temperature drops rapidly, then slowly rises, and near the nozzle, the temperature rises again rapidly. The monitoring line is on the boundary line between the innermost grid of the wall and the outermost grid of the gas, so the temperature value here is the average of the gas temperature and the wall temperature.

At the inlet, the temperature boundary layer of the gas is not formed, so the average temperature is higher. Subsequently, due to the temperature boundary layer, the near-wall gas temperature is significantly lower than the mainstream gas temperature, resulting in a decrease in the average temperature.

DOI: 10.13009/EUCASS2019-373



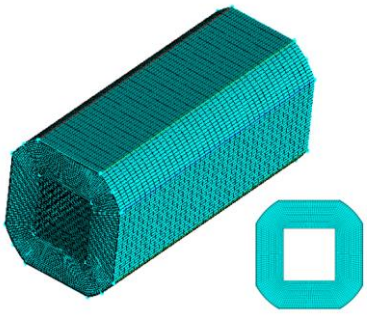

Figure 3: the mesh of the solid part

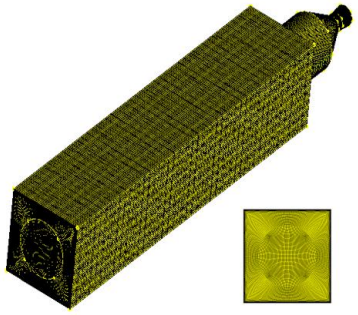

Figure 4: the mesh of the gas part

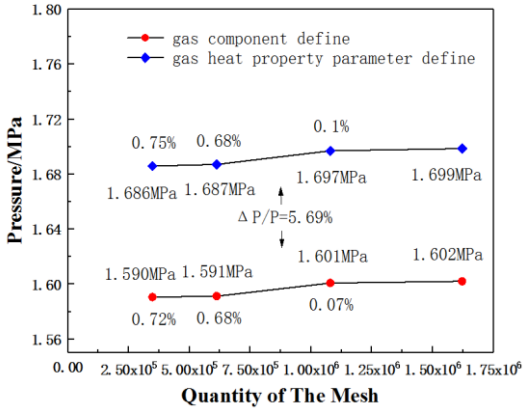


Figure5 Mesh independence analysis (according to the pressure)

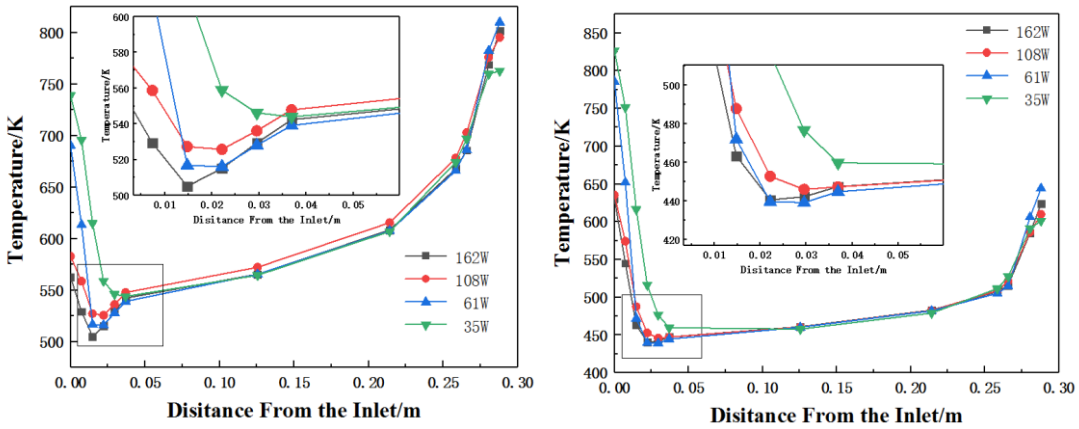


(a)gas component defined (b)gas heat property parameter defined

Figure6 Mesh independence analysis (according to the temperature)

### 3.2 Numerical simulation results

The temperature at 1 micron (within the first grid) in the wall is selected to represent the wall temperature, and the wall temperature as a function of time is shown in Fig. 7. During the simulation, the monitored point distances are shown in Table 3. At the same time, by monitoring the temperature of the point at the same axial position as point 3 and point 5 but at a distance of 2 mm and 4 mm from the gas wall, and using Fourier's law (9), the heat flow value

DOI: 10.13009/EUCASS2019-373



and point 3 and point 5 can be derived. The temperature value is shown in Figure 8.

$$q = \frac{\lambda}{\delta} \Delta T \tag{9}$$

It can be seen from Fig. 7 that whether the gas thermal property parameter is defined or the gas component is defined, the wall temperature gradually decreases from the inlet to the outlet. The heat flow distribution calculated by monitoring the temperature at points at different depths also conforms to this rule. The reason for this phenomenon is that the temperature boundary layer is not completely formed at the inlet, so that the temperature of the gas near the wall at the inlet is higher, and then the temperature rises faster.

Table 3: the distance of the monitoring points from the inlet

| **The number of the point** | **The distance from the inlet/mm** |
|---|---|
| 1 | 30 |
| 2 | 68 |
| 3 | 106 |
| 4 | 144 |
| 5 | 182 |
| 6 | 220 |
| 7 | 258 |

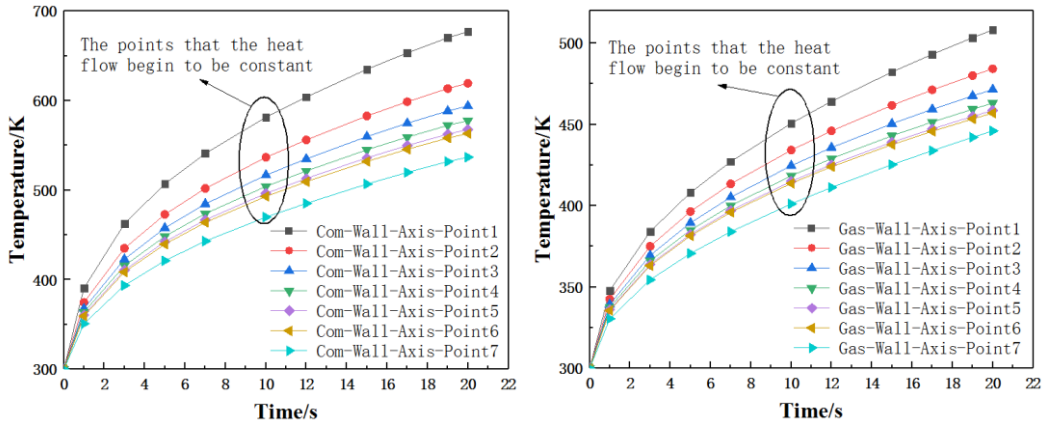


(a)gas component defined (b)gas heat property parameter defined

Figure 7: the temperature of the monitoring points

DOI: 10.13009/EUCASS2019-373



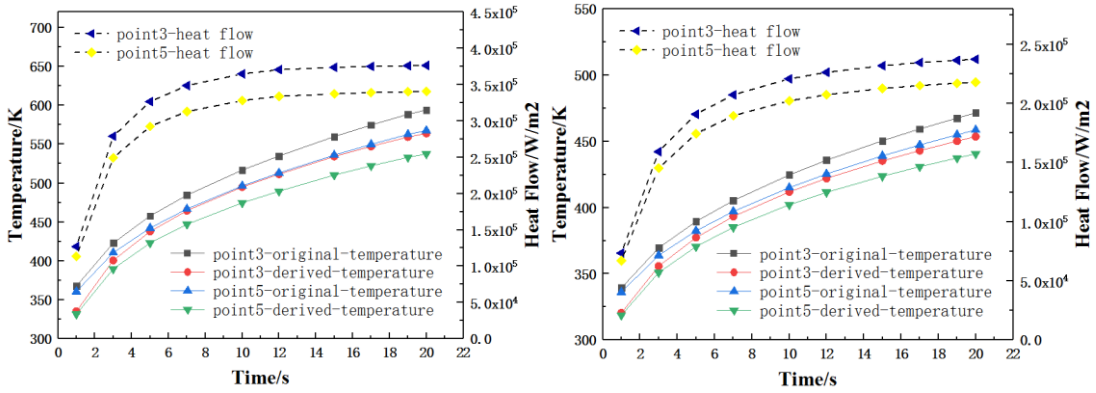


(a)gas component defined (b)gas heat property parameter defined

Figure 8: the calculated heat flow and the temperature of point3 and point5

Due to the gradual formation of the temperature boundary layer, the gas temperature near the wall Basically unchanged, the temperature at the monitoring point in the middle is getting slower and slower toward the entrance, and the temperature at the last monitoring point is more severe. This is due to the presence of a boss at the rear end of the engine.

The cloud map shows that the appearance of the boss causes the temperature boundary layer at the tail to thicken, which in turn affects the temperature at that point. However, since the position of the point 7 is still a certain distance from the tail boss, the effect of the temperature rise due to the local temperature rise caused by the gas stagnation is not so significant. It can also be seen from Fig. 7 that at 10s, the temperature change of the engine wall tends to be linear, which indicates that the heat transfer from the gas to the wall tends to be constant at this time. It can be seen intuitively from Fig. 8 that at 10s, the heat flow value tends to be constant, which is consistent with the conclusions obtained in Fig. 7. At the same time, Figure 8 also shows that the temperature of the axial monitoring point calculated by Fourier's law is lower than the temperature of the monitoring point, and the difference is about 15K. This is because at the same time, the temperature distribution at the same axial position is not linear with the radial position. The closer the temperature difference is to the inner wall of the engine, the more the temperature should be reversed when using the temperature at different depth points.The wall temperature cloud map, the gas temperature cloud map, and the heat flow transmitted by the gas to the wall are calculated as shown in Figs. 9, 10, and 11.

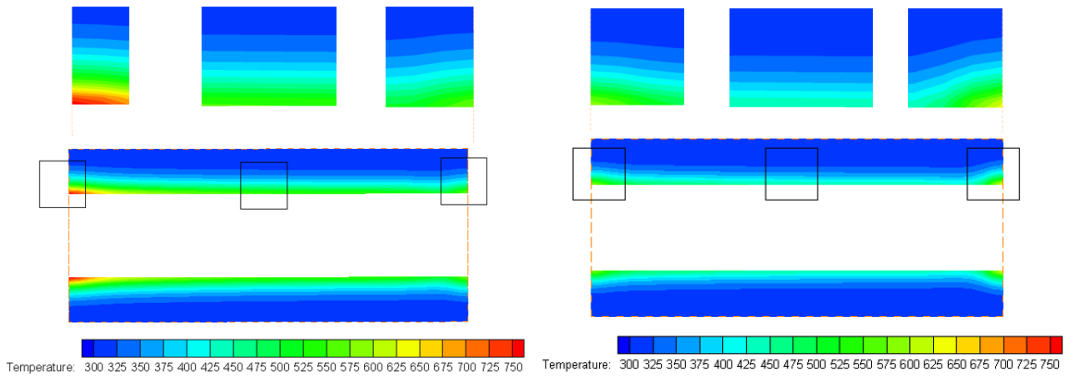


(a)gas component defined (b)gas heat property parameter defined

Figure 9: the temperature field cloud picture of the solid

DOI: 10.13009/EUCASS2019-373



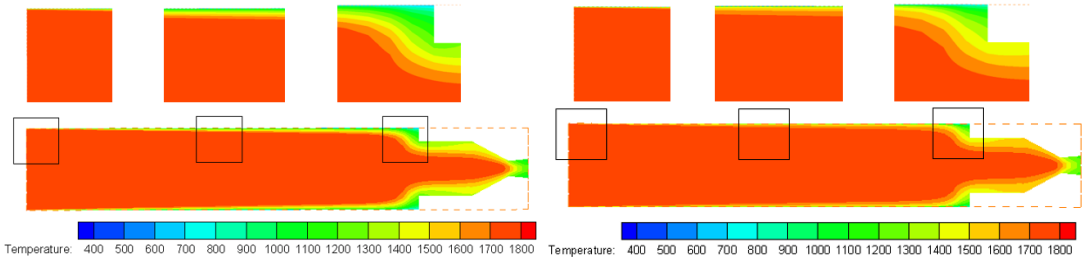


(a)gas component defined (b)gas heat property parameter defined

Figure 10: the temperature field cloud picture of the gas

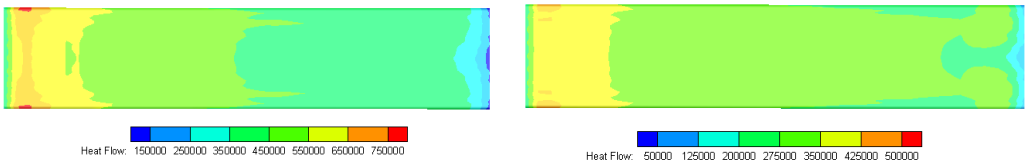


(a)gas component defined (b)gas heat property parameter defined

Figure 11: the heat flow field cloud picture of the couple wall

It can be clearly seen from Fig. 9 that the temperature rise in the front section of the engine casing is faster, the middle part is relatively slow, the tail is re-accelerated, and the development of the gas temperature boundary layer along the axial direction and the tail due to the boss. Local temperature changes caused by flow stagnation. As can be seen from Fig. 11, the heat flow value gradually decreases from the inlet and is significantly lower at the extreme end, mainly due to the thicker gas temperature boundary layer here, as shown in Fig. 10.

It can also be seen from the simulation results that the gas-to-wall heat transfer obtained by the calculation of the gas component is significantly higher than the definition of the gas thermal property parameter. This is mainly due to the fact that when the gas component is defined for calculation, the thermal conductivity of the mixed gas is calculated by weighting the thermal conductivity of various gases, instead of being considered as a function of temperature. As a result, the coefficient is higher(0.0757W/(m Ⱪ)), which is higher than the value(0.031 W/(m Ⱪ)) calculated by CEA.

## 4. Thermal test experiment research

In order to obtain more accurate engine wall heating conditions, two experiments were carried out in this study. The experimental conditions are shown in Table 4. The experimental system of this experiment is shown in Figure 12. In the experiment, the orifice was used for current limiting to obtain the flow rate of the desired oxidant and fuel. At this part, the wall temperatures of the point1-7 are measured by the thermocouples. And the heat flow of point3 and point5 are measured by the intelligent heat flow meter. The pressure of the combustion chamber can prove that the rocket engine is working normally. And the other pressure of the experimental system can prove that the mass flows of the oxygen and fuel are as expected.

DOI: 10.13009/EUCASS2019-373



Table 4: experimental conditions

| The name of the parameters | The number of the parameters |
|---|---|
| Pc/MPa | 1.7 |
| Mass flow/g/s | 120 |
| O/F | 1 |
| Throat diameter/mm | 12 |
| Carbon deposit | Case A: no<br>Case B: yes |

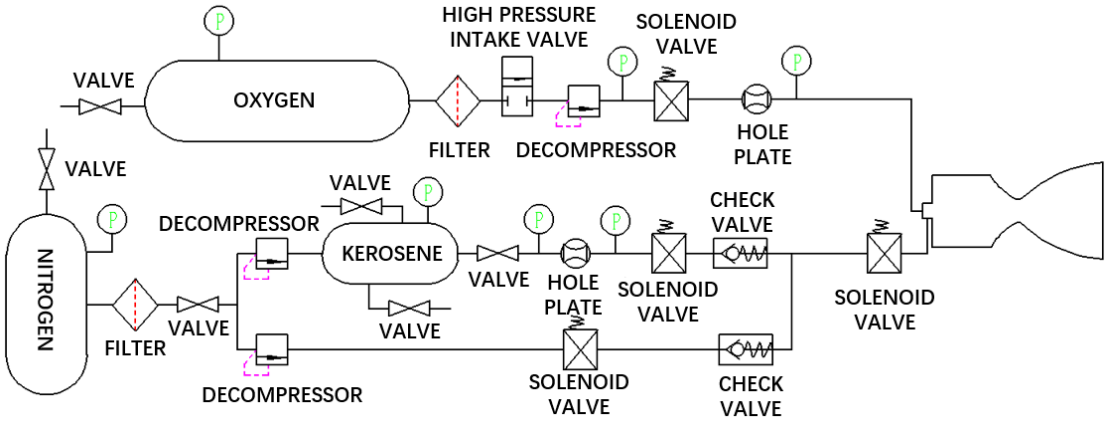


Figure 12: experimental device system

### 4.1caseA

By monitoring the pressure of the fuel tank, the pressure before and after the orifice, the pressure before injection and the pressure of the oxygen tank, the pressure before and after the hole plate, and the pressure before injection, it is judged whether the supply system has achieved the function of stably supplying fuel and oxygen. In the normal working section of the combustion chamber, the pressure of the oxygen storage tank decreases linearly, and the remaining pressure values remain constant. During the test, the chamber pressure value was monitored to be 1.4 MPa, which was lower than the design value. This was mainly due to the heat transfer in the actual process, resulting in a decrease in gas pressure in the combustion chamber.

DOI: 10.13009/EUCASS2019-373



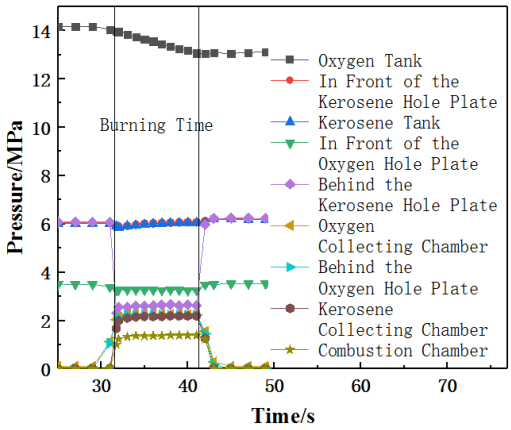


Figure 13: The main pressure monitoring points

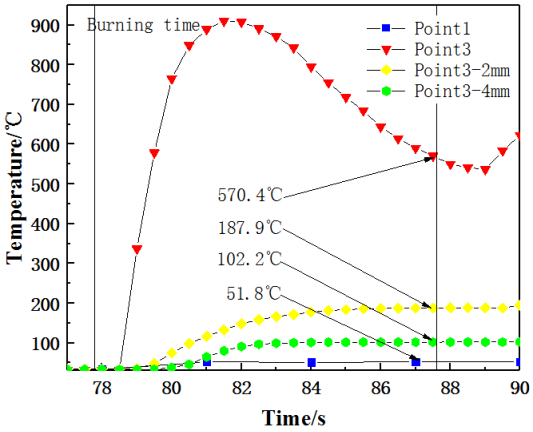


Figure 14: The temperature of the point1,3

The experiment found that the temperature at point1 reached stable operation shortly after the normal operation of the engine. The measured temperature was 51.8 ℃ at equilibrium. This is mainly because the axial distance of point1 is the mixing and atomization stage of the engine, so the temperature is low. While the temperature measured by point3 is higher, and the temperature is still not stable when the engine is finished, which is much higher than the temperature obtained by Fourier's law, about 300 ℃. This is mainly because the thermocouple has protruded into the gas by about 1 mm, causing that the measured temperature is not the wall temperature.

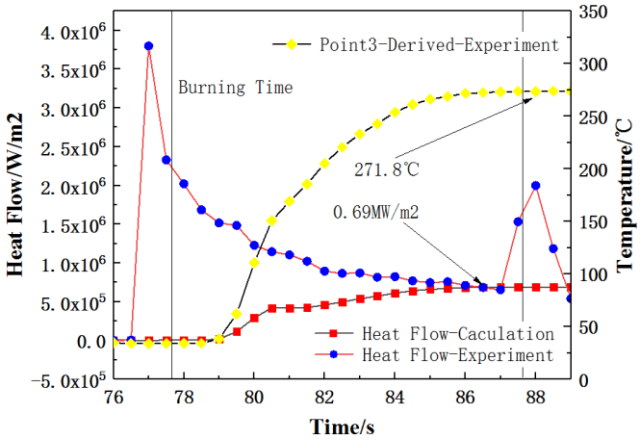


Figure 15: The heat flow and the derived temperature of point3

It can be seen from the test of the heat flow densitometer and the calculation using Fourier's law that the heat flow is close to approximately 10 s, and the measured heat flow value is about 0.69 MW/m$^2$ .

### 4.2caseB

Considering that there is a large amount of carbon generated when the engine is working. In order to analyse the effect of carbon deposition on the heat transfer of the gas, under the same working conditions, the experiment is carried out again, and the working time of the combustion chamber is extended to 15s. The pressure data is shown in the figure. According to the experimental data, it is easy to see that in the working stage, the fuel and oxidant flow rate is basically stable, and the pressure in the combustion chamber is 1.5 MPa. Compared with the previous

DOI: 10.13009/EUCASS2019-373



experiment, the pressure is slightly increased, This is because the amount of external heat transfer is small.

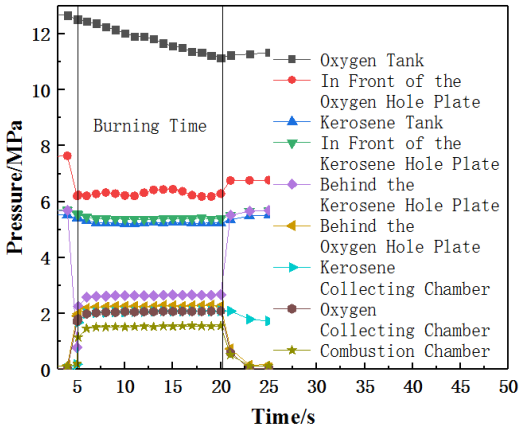


Figure 16: The main pressure monitoring

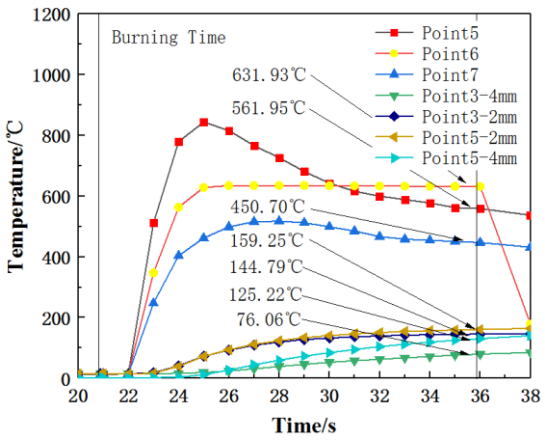


Figure 17: The temperature of the point3,5-7

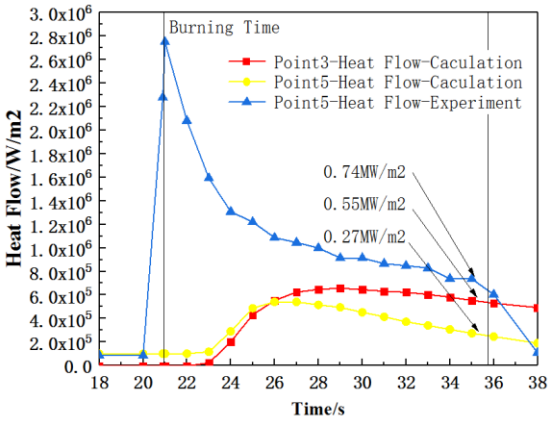


Figure 18: The heat flow point3、5

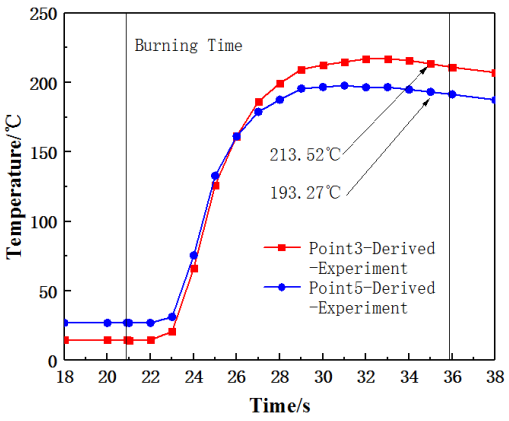


Figure 19: The derived temperature of point3、5

The temperature data mainly monitored in this experiment is shown in the figure. It can be seen from the temperature trend in the figure17 that the position of the thermocouple head is well controlled that almost all of them are near the wall surface, only point 5 is slightly higher than the wall surface, because it penetrates into the gas. Point 7 is in the wall and is not completely exposed, resulting in the lower temperature.

In this experiment, the point 5 point heat flow value measured by the heat flow densitometer is 0.74 MW/m$^2$, which is slightly higher than 0.69 MW/m$^2$ in the previous experiment, indicating that between point 3 and point 5, the reaction in the combustion chamber is further carried out, and the heat release is further increased. . However, it is easy to see that the heat flow at the point 3 and 5 is 0.55 MW/m$^2$ and 0.27 MW/m$^2$ calculated by using Fourier's law. The existence of carbon deposition leads to the reduction of gas-to-wall heat transfer, and the closer to the tail of the engine, the product The more serious the carbon.

### 4.3 Comparative analysis

In the first experiment, Fourier's law and the measured temperatures of two different depth points were used to estimate the engine gas wall surface temperature. It was found that when the value was stable, the temperature at point3 reached 271.8 ℃. In the second experiment, the temperature at point 5 was directly obtained at 561.95 ℃.

DOI: 10.13009/EUCASS2019-373



Using these two temperatures, the theoretical calculations of the heat flow values at point 3 and point 5 are calculated to be 0.76 MW/m$^2$ using the Bartz formula, indicating that the 650K assumption is reasonable in this study, but The theoretically calculated value is a little large.

It can be seen from the comparison between experiment and simulation that the experimental heat flow (0.69 MW/m$^2$ at point3 and 0.74 MW/m$^2$ at point5) is significantly higher than the simulation result (0.22 MW/m$^2$ at point3 and 0.24 MW/m$^2$ at point5). Mainly because the influence of carbon deposition on heat transfer is neglected in the simulation, the carbon deposition attached to the wall of the combustion chamber will additionally introduce heat conduction heat flow, and the generation of carbon particles will increase the blackness of the gas and engine wall, and further increase the radiant heat flow.

## 5 Conclusion

In this paper, the effects of gas on the wall surface heat transfer of rich coal-fired oil-gas oxygen liquid rocket engine are studied by using theoretical calculation, simulation research and experimental research. The research finds:

(1) The 650K wall temperature assumption used in the theoretical calculation is reasonable while the calculated heat flow value is 0.78 MW/m$^2$, which is almost the same as the calculation(0.76 MW/m$^2$) when the experimentally measured wall temperatures at point 3 and point 5 are introduced. And the value is slightly higher than the value measured by the experiment;

(2) Simulation calculation When the gas component is defined, the gas thermal conductivity is prone to be high, which will lead to the increase of gas to the wall. Therefore, Using the CEA calculation first, and then defining the gas thermal property parameter is reasonable;

(3) For the research object of this paper, the fuel-fired oil-gas oxygen liquid rocket engine is simply calculated by the simulation calculation of the gas thermal property parameters, which is far from the actual situation, which mainly ignores the influence of carbon deposition;

(4) It is also found that carbon deposition can effectively reduce the heat transfer of gas to the engine wall, and the closer to the nozzle, the more serious the carbon deposit, the more obvious this effect.

## References

[1] Lai Y G, Przekwas A J, Nguyen N. A Concurrent MuIti-dsicipIinaryApproach for the AnaIysis of Liguid Rocket Engine Combustors[R]. AIAA 94-3103, 1994.

[2] Xiaowei wang, Ping Jin, Guobiao Cai, et al. Method for measurement of single injector heat transfer characteristics[J]. Journal of propulsion technology, 2008, 29(6): 726-732.

[3] Xiaowei wang, Ping Jin, Guobiao Cai, et al. Method for investigation of combustion flow field characteristic in single element gas/gas injector chamber[J]. Journal of Beijing University of Aeronautics and Astronautics, 2009, 35(9) :1095-1099.

[4] Marco Pizzarelli , Barbara Betti . et al. Coupled analysis of hot-gas and coolant flows in LOX/methane thrust chambers[C]. 4th European Conference For Aerospace Science, 2011.

[5] Betti B, Pizzarelli M, Nasuti F. Coupled Heat Transfer Analysis in Regeneratively Cooled Thrust Chambers[J]. Journal of Propulsion and Power, 2014,30(2):360-367.

[6] M.P.Celano , S.Slivestri , J.Pauw . et al. Heat Flux Evaluation Methods for a Single Element Heat-Sink Chamber[C]. 6th European Conference For Aerospace Science, 2015.

[7] D.Suslov , B. Betti , T.Aichner . et al. Experimental Investigation and CFD-Simulation of the Film Cooling in an O2/CH4 subscale Combustion Chamber[C]. 7th European Conference For Aerospace Science, 2017.

DOI: 10.13009/EUCASS2019-373



[8] Peter C. Ma , Hao Wu , Matthias Ihme , et al. A flamelet model with heat-loss effects for predicting wall-heat transfer in rocket engines[C]. 53rd AIAA/ASME/SAE/ASEE Joint Propulsion Conference, 2017.

[9] Lina Peng. Analysis and test of thermal protection of RBCC main rocket and combustion chamber[D].Northwesten Polytechnical University, 2007.

[10]Linshun Di, Dingyou Fang, Deyi Ma. Rocket engine principle, University of national defense science and technology of the people's liberation army.

[11]Zhongli Zhang, Mengzheng Zhang, Lixin Zhou. Thermal protection of liquid rocket engines [M].Beijing : National defense industry press, 2016.

[12]Shiming Yang, Wenshuang Tao. Heat transfer [M].Beijing : Higher education press, 2006.

[13]Lijun Yang, Qingfei Fu. Design of thrust chamber for liquid rocket engine [M]. Beijing : Beijing university of aeronautics and astronautics press, 2013.